CDF note 11098

Measurement of the W^+W^- Production Cross Section and Differential Cross Sections with Jets in $p\bar{p}$ Collisions at $\sqrt{s} = 1.96$ TeV

The CDF Collaboration
URL http://www-cdf.fnal.gov
(Dated: June 19, 2014)

W^+W^- production is an interesting process in the gauge sector being produced both by radiation from quarks and multiple gauge boson coupling. It is also a critical background for measurements of Higgs production with decay to WW bosons. We report a new measurement of the W^+W^- production cross section in the two charged lepton (e, μ), two neutrino, and n jet final state in $p\bar{p}$ collisions at a center of mass energy of 1.96 TeV. The data were collected with the CDF II detector at the Tevatron collider at Fermilab and uses the full 9.7fb^{-1} CDF dataset. A neural net is trained to distinguish W^+W^- signal from background. The W^+W^- cross section is then extracted using a maximum likelihood method to fit the W^+W^- and background neural net shapes. The W^+W^- cross section is presented both inclusive and differentially in jet multiplicity. We additionally subdivide the one jet region by leading jet E_T. The measured cross section is $14.0 \pm 0.6(stat)^{+1.6}_{-1.3}(syst) \pm 0.8(lumi)$ pb.

I. INTRODUCTION

The direct production of $W^+W^-(WW)$ pairs in proton-antiproton collisions is the primary background in searches for a high mass Standard Model Higgs boson decaying to WW. A good understanding and modeling of WW production is thus essential to any Higgs to WW search. This measurement is an offshoot of the Standard Model $H \to WW \to ll\nu\nu$ search described in Phys. Rev. D 88 [21], using the same framework and selection. The WW cross section has been measured previously at CDF[6] with 3.6fb^{-1} of data and D0[12] with 1fb^{-1} of data as well as at the LHC [11],[5]. We consider events with two leptons (e or μ) and substantial $\not\!\!E_T$. Considering WW events with jets in the final state provides a unique test of QCD calculations of states with two vector bosons and multiple associated jets. In separate bins we measure the cross section for events with zero jets, with one jet of $15 < E_T < 25$ GeV, with one jet of $25 < E_T < 45$ GeV, with one jet of $E_T > 45$ GeV, and with two or more jets. We train NeuroBayes®neural nets to separate WW events from background, and fit the neural net output templates using a binned maximum likelihood method to extract the WW production cross section. Our result is the most precise measurement of the WW production cross section at a $p\bar{p}$ collider.

II. DETECTOR DESCRIPTION

The components of the CDF II detector relevant to this anlaysis are described briefly here; a more complete description can be found elsewhere [7]. The detector geometry is described by the azimuthal angle ϕ and the pseudo-rapidity $\eta \equiv -\ln(\tan\theta/2)$, where θ is the polar angle of a particle with respect to the proton beam axis (positive z-axis). The pseudo-rapidity of a particle originating from the center of the detector is referred to as η_{det}. The trajectories of charged particles are reconstructed using silicon micro-strip detectors [8][9] and a 96-layer open-cell drift chamber (COT[10]) embedded in a 1.4 T solenoidal magnetic field. For $|\eta_{det}| \leq 1$, a particle traverses all 96 layers of the COT; this decreases to zero at $|\eta_{det}| \approx 2$. The silicon system provides coverage with 6(7) layers with radii beetween 2.4 cm and 28 cm for $|\eta_{det}| < 1.0$ ($1.0 < |\eta_{det}| < 2.0$). Outside of the solenoid are electromagnetic (EM) and hadronic (HAD) sampling calorimeters segmented in a projective tower geometry. The first hadronic interaction length (λ) of the calorimeter, corresponding to 19-21 radiation lengths (X_0), uses lead absorber for measuring the electromagnetic component of showers, while the section extending to 4.5-7 λ uses iron to contain the hadronic component. The calorimeters are divided in a central ($|\eta_{det}| < 1$) and forward ($1.1 < |\eta_{det}| < 3.64$) region. Shower maximum detectors (SMX) embedded in the electromagnetic calorimeters at approximately $6X_0$ help in the position measurement and background suppression for electrons. Outside of the central calorimeters are scintillators and drift chambers for identifying muons as minimum ionizing particles. We use three complementary track patter recognition algorithms which are distinguished by their starting point in COT, silicon, or projection from calorimeter energy cluster to interaction region.

III. LEPTON IDENTIFICATION

In order to maximize signal acceptance and suppress backgrounds from jets and photons misidentified as leptons we use two (eight) categories of electrons (muons). Two additional categories, based on central tracks that are not fiducial to calorimeters or muon detectors, are used as either an electron or muon in forming WW candidates. The resulting categories exploit essentially all the tracks and electromagnetic calorimeter clusters available. All leptons are required to be isolated such that the sum of the E_T for the calorimeter towers in a cone of $\Delta R = \sqrt{(\Delta\eta)^2 + (\Delta\phi)^2} < 0.4$ around the lepton is less than 10% of the electron E_T or muon p_T. If an additional good muon or electron candidate is found within the $\Delta R < 0.4$ cone, the towers the additional lepton passed through are subtracted from the E_T sum. The transverse energy E_T of a shower or calorimeter tower is $E\sin\theta$, where E is the associated energy. Similarly, p_T is the component of track momentum transverse to the beam line. Electron candidates are required to have a HAD energy to EM energy consistent with originating from an electromagnetic shower and are further divided into central and forward categories. The central electron category requires a well-measured COT track satisfying $p_T > 10$ GeV/c that is fiducial to the central SMX and matched to a central EM energy cluster. Central electron candidates are then selected for which shower shape and energy deposition are consistent with an electron, or by using a likelihood method to combine electron identification variables into one discriminant. A forward electron is required to be fiducial to the forward SMX detector and have energy deposition in both the calorimenter towers and SMX detector consistent with an electron shower shape. For each forward candidate, we also require a matching calorimeter seeded track that is consistent with a standalone reconstructed track formed using hits in the silicon detector to reduce background from photons. Alternatively, a forward electron can also be included if it passes a likelihood based discriminant based on similar variables. Muons are identified by either a charged track matched to a reconstructed track segment ("stub")

in muon chambers or as a stubless minimum ionizing particle fiducial to calorimeters. In addition, stubless muons are required to have at least 0.1 GeV in total calorimeter energy. For $|\eta_{det}| < 1.2$, strict requirements on the number of COT hits and the χ^2 of the track fit are placed on the muon tracks in order to suppress kaon decay-in-flight backgrounds. The category of stubless muons with $|\eta_{det}| > 1.2$ requires that at least 60% of the COT layers crossed by the track have hits. In order to suppress background from cosmic rays, the track's point of closest aproach to the beamline must be consistent with originating from the beam. The final category of leptons are constructed from tracks which are not fiducial to the SMX detectors nor identified as stubbed muons. The requirements for the tracks are the same as stubless muons with $|\eta_{det}| < 1.2$, but without any of the calorimeter requirements. Due to the lack of calorimeter information, electrons and muons cannot be reliably differentiated in this region, and this category is therefore treated as having either flavor in the WW candidate selection. If an electron or non-fiducial track candidate is consistent with being due to a photon conversion as indicated by the presence of an additional nearby track, the candidate is vetoed. To identifiy the presence of W bosons decaying to two neutrinos, we use the missing transverse energy $\not\!\!E_T = |\Sigma_i E_{T,i}\hat{\eta_{T,i}}|$, where the $\hat{\eta_{T,i}}$ is the transverse component of the unit vector pointing from the interaction point to calorimeter tower i. The $\not\!\!E_T$ is corrected for muons which do not deposit all of their energy in the calorimeter and tracks which point to uninstrumented regions of the calorimeter. The WW candidate events are required to pass one of five online trigger selections implemented in three successively more stringent levels. The final central electron requirement is an EM energy cluster with $E_T > 18$ GeV matched to a track with $p_T > 8$ GeV/c. Muon triggers are based on information from muon chambers matched to a track wtih $p_T > 18$ GeV/c. The trigger for forward electrons requires an $E_T > 20$ GeV EM energy cluster and an online measurement of the $\not\!\!E_T > 15$ GeV.

IV. EVENT SELECTION

The $ll\nu\nu$ candidates are selected from two opposite-sign leptons. At least one lepton is required to satisfy the trigger and have $E_T > 20$ GeV ($p_T > 20$ GeV/c) for electrons (muons). We loosen this requriement to > 10 GeV (GeV/c) for the second lepton to increase WW kinematic acceptance. The z-positions of the leptons in a candidate at the point of closest approach to the beam-line are required to be within 4 cm of each other. There are several sources of background: W+jets and $W\gamma$ where a jet or photon is misidentified as a lepton, Drell-Yan where $\not\!\!E_T$ is large due to mismeasurement of lepton or jet E_T, $t\bar{t} \to b\bar{b}ll\nu\nu$, and WZ and ZZ where one or two leptons are lost or one boson decays hadronically. To suppress W+jets and $W\gamma$ we apply an isolation requirement that the sum of track p_T in a cone of $\Delta R < 0.4$ around each cut-based lepton is less than 10% of the electron E_T or muon p_T. We also require event candidates to have $m_{ll} > 16$ GeV/c^2. To suppress Drell-Yan we define the variable $\not\!\!E_{Tspec}$:

$$\not\!\!E_{Tspec} \equiv \begin{cases} \not\!\!E_T & \text{if} \Delta\phi(\vec{\not\!\!E_T}, lepton, jet) > \frac{\pi}{2} \\ \not\!\!E_T sin(\Delta\phi(\vec{\not\!\!E_T}, lepton, jet) & \text{if} \Delta\phi(\vec{\not\!\!E_T}, lepton, jet) < \frac{\pi}{2} \end{cases} \quad (1)$$

This measures the transverse component of $\not\!\!E_T$ relative to the closest lepton or jet in an event. We require it to be > 25 GeV (15 GeV for electron-muon events, for which the Drell-Yan background is inherently smaller). Due to large Drell-Yan systematic uncertainties we make two additional cuts. We veto events with m_{ll} between 80 and 99 GeV (unless they are identified as electron-muon events), reducing $Z \to ee$ and $Z \to \mu\mu$ events. We also veto events where $\Delta\phi$ between the $\not\!\!E_T$ and the vector sum of the lepton momenta is > 1. This greatly reduces the contribution from $Z \to \tau\tau$ events. To suppress $t\bar{t}$ background we veto events with two or more jets in which one or more jets is b-tagged by HOBIT[23]. To suppress WZ and ZZ we require exactly two leptons in the final state. We consider separately final states with zero, one, or two or more jets in the final state, where a jet is required to have $E_T > 15$ GeV and $|\eta < 2.5$. The expected and observed yields after base selection cuts have been applied are shown for each jet region in Table I.

V. DATA MODELING

The geometric and kinematic acceptance for the WW signal and the Drell-Yan (DY), WZ, ZZ, $W\gamma$, and $t\bar{t}$ backgrounds are determined using a Monte Carlo simulation of the collision interfaced to a Geant3-based simulation of the CDF II detector [20] reponse. The WW sample and DY two or more jets sample are generated in Alpgen [19] and showered in Pythia. The $W\gamma$ sample is generated with Baur MC [2]. The remaining processes, (DY 0 and 1 jet, WZ, ZZ, $W\gamma$, and $t\bar{t}$) are simulated with Pythia [24]. We use the CTEQ5L [15] parton distribution functions (PDFs) to model the momentum distribution of the initial-state partons. A number of corrections are applied to the Monte Carlo. Lepton reconstruction and identification efficiencies are measured in data using Z decays. A correction of up to

WW(ll$\nu\nu$) Cross Section CDF Run II Preliminary $\int \mathcal{L} = 9.7$ fb^{-1}			
Process	Events (Best Fit)		
	0 Jets	1 Jet	2 or More Jets
WZ	19.5 ± 3.0	16.7 ± 2.3	4.26 ± 0.81
ZZ	13.2 ± 1.9	4.25 ± 0.61	1.33 ± 0.26
$t\bar{t}$	3.7 ± 1.0	76 ± 12	158 ± 16
DY	150 ± 34	83 ± 21	20.2 ± 8.6
$W\gamma$	214 ± 27	44.0 ± 6.4	7.5 ± 1.9
W+jets	685 ± 118	250 ± 46	81 ± 15
Total Background	1086 ± 124	474 ± 57	272 ± 26
WW	963 ± 108	224 ± 29	73 ± 20
Signal+Background	2049 ± 177	698 ± 73	345 ± 39
Data	2090	682	331

TABLE I: Predicted and observed event yields in the signal region.

10% per lepton (depending on lepton type) is applied. An additional 10% correction is applied to muons reconstructed from minimum ionizing energy deposits in the forward calorimeter to account for known poor modeling of the track reconstruction in this region. A 31% correction is applied to the $W\gamma$ background estimate derived from a study of the low-m_{ll} $W\gamma$ control region [14]. $t\bar{t}$ is normalized to a measurement of the $t\bar{t}$ cross section in the dilepton channel[22]. In the two or more jet region, an additional scale factor of 1.03 is applied to the $t\bar{t}$ background to account for a small number of events for which the silicon micro-strip detectors required for b-tagging were not operational. Trigger efficiencies are determined from $W \to e\nu$ data for electrons and from $Z \to \mu^+\mu^-$ data for muons. The background from W+jets is estimated from a sample of events with an identified lepton and a jet that is required to pass loose isolation requirements and contain a track or energy cluster similar to those required in the lepton identification. The contribution of each event to the total yield is scaled by the probability that the jet is identified as a lepton, as determined from multijet events collected with jet-based triggers at a variety of energy thresholds. A correction is applied for the small real lepton contribution using single W and Z bosons Monte Carlo simulation.

VI. CONTROL REGIONS

We define several control regions to validate our background modeling. An example of the agreement in each region is found in Figure 1. To validate our modeling of Drell-Yan we consider opposite sign leptons in the Z mass region $76 < m_{ll} < 106$ GeV. We veto electron-muon events, and relax the $\not\!\!E_{Tspec}$ cut to $15 < \not\!\!E_{Tspec} < 25$ GeV. We generally observe good agreement with Monte Carlo. A discrepancy in the Njets distribution is accounted for by $\not\!\!E_T$ modeling and jet energy scale systematic uncertainties discussed below. We further subdivide the Drell-Yan region by jet multiplicity and verify that no further discrepancies exist. To validate W+jets and $W\gamma$ modeling, we reverse the opposite sign requirement on the signal selection criteria, resulting in a region dominated by fake leptons originating from either jets or photons. We observe good agreement with Monte Carlo. To validate our modeling of $t\bar{t}$ events we reverse the btag veto in the two or more jet region, requiring at least one b-tagged jet. Since the region is nearly pure $t\bar{t}$ we relax the dimass and $\Delta\phi(ll, \not\!\!E_T)$ cuts that are intended to suppress Drell-Yan.

VII. CROSS SECTION MEASUREMENTS

For each signal region, we train an independent NeuroBayes®neural network on signal and background Monte Carlo events. Each neural net has three layers consisting of input nodes, hidden nodes, and one output node. Templates are created from the trained neural net that serve as the final discriminant in calculating the cross section. We separate the one jet neural net into three templates, corresponding to $15 < E_T < 25$ GeV, $25 < E_T < 45$ GeV, and $E_T > 45$ GeV and fit each template independently.

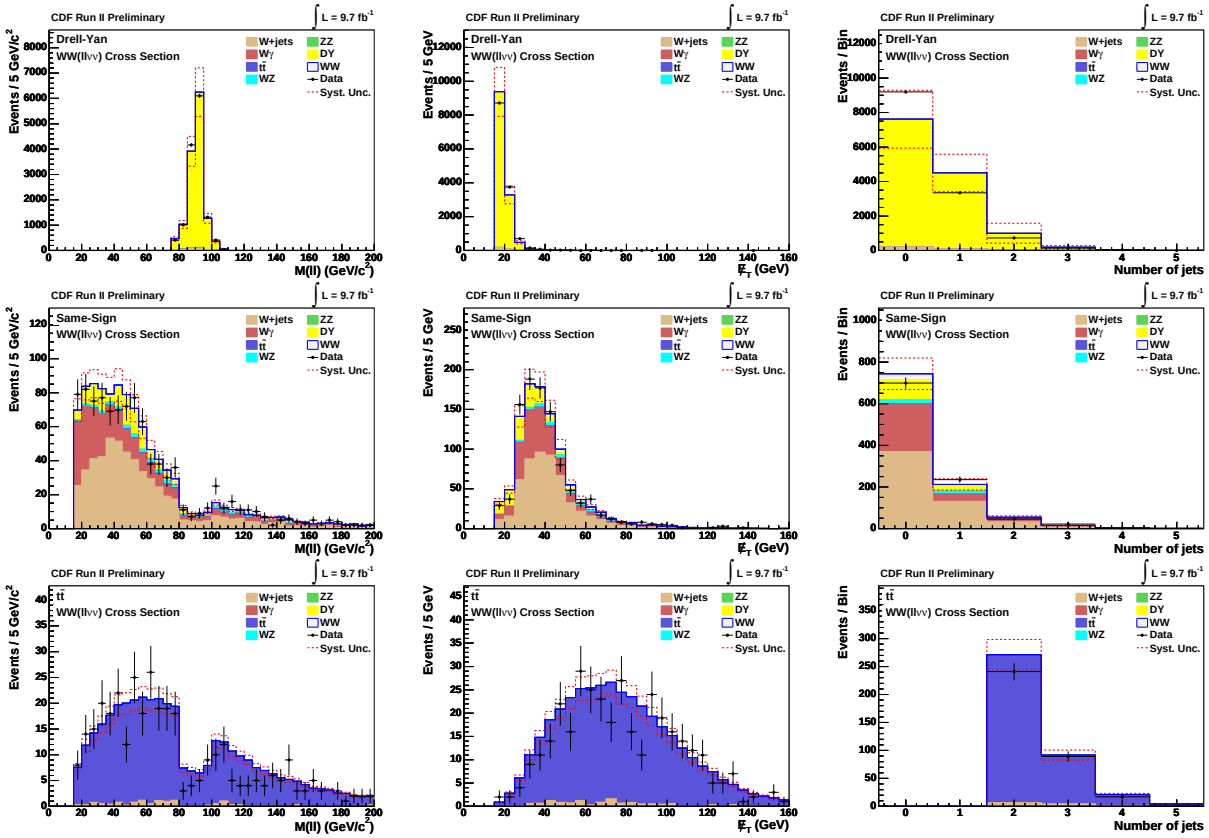

FIG. 1: Examples of agreement in control regions. From top to bottom: Drell-Yan, Same Sign, and $t\bar{t}$.

A. Zero Jet Analysis

The zero jet analysis uses nine input variables. The inputs are the scalar sum of the lepton transverse energies and $\not\!\!E_T$; the p_T of the subleading lepton; the likelihood ratio for WW production; the invariant mass of the two leptons; $\Delta\phi$ between the two leptons; the transverse mass of the sum of the lepton momenta and $\not\!\!E_T$; the p_T of the leading lepton; the energy of the leading lepton; and ΔR between the leptons. The likelihood variables were calculated on an event by event basis using leading order matrix elements from the MCFM [4] package. Probability densities were calculated for four processes: WW, WZ, $W\gamma$, and W+jets according to the formula

$$P(\vec{x_{obs}}) = \frac{1}{\langle\sigma\rangle}\int \frac{d\sigma_{th}(\vec{y})}{d\vec{y}}\epsilon(\vec{y})G(\vec{x_{obs}},\vec{y})d\vec{y} \tag{2}$$

where the variables are as follows

- $\vec{x_{obs}}$ - observed lepton momenta and $\not\!\!E_T(x,y)$
- $\vec{y}$ - true lepton 4-vectors (including neutrinos)
- σ_{th} - leading order theoretical cross section
- $\epsilon(\vec{y})$ - efficiency and acceptance for the event
- $G(\vec{x_{obs}},\vec{y})$ - an analytic model of detector resolutions effects
- $1/\langle\sigma\rangle$ - normalization

The function $\epsilon(y)$ describes the probabilities of a parton level object (e, μ, γ, or parton) to be reconstructed as one of the lepton categories. The efficiency function is determined solely from Monte Carlo for e and μ, and from a combination of Monte Carlo and data-driven measurements described in Section V for γ and partons. A discriminant is constructed from the event probability densities:

$$LR_{WW} = \frac{P_{WW}}{P_{WW} + \sum_i k_i P_i} \tag{3}$$

where k_i is the expected fraction for each background and $\Sigma_i k_i = 1$. The neural net input templates are shown in Figure 2.

B. One Jet Analysis

The one jet analysis uses 8 input variables. The inputs are the scalar sum of the lepton transverse energies and $\not\!\!E_T$; the p_T of the subleading lepton; the $\not\!\!E_{Tspec}$; the energy of the leading lepton; ΔR between the leptons; the transverse mass of the sum of the lepton momenta and $\not\!\!E_T$; the p_T of the leading lepton; and the invariant mass of the two leptons. We do not use likelihood ratios in the one or two jet regions as they would be computationally intensive to calculate. The neural net input templates are shown in Figure 3.

C. Two or More Jets Analysis

The two or more jet analysis uses 17 input variables. The inputs are the scalar sum of the lepton transverse energies and $\not\!\!E_T$; the vector sum of the first and second jet p_T; the $\not\!\!E_{Tspec}$; the p_T of the subleading lepton; the $\not\!\!E_{Tsig}$; the aplanarity; the transverse mass of the sum of the lepton momenta and $\not\!\!E_T$; the ΔR between the leptons; the scalar sum of the lepton and jet E_Ts; the transverse mass of the sum of the lepton and jet momenta and $\not\!\!E_T$; the $\cos(\Delta\phi)$ between leptons in the WW CM frame; the $\Delta\phi$ between the vector sum of lepton momenta and $\not\!\!E_T$; the scalar sum of jets E_T and $\not\!\!E_T$; the invariant mass of the two leptons; the p_T of the leading lepton; the cos of the angle between the second lepton and WW momentum; and $\Delta\phi$ between the leptons. We do not use likelihood ratios in the one or two jet regions as they would be computationally intensive to calculate. The neural net input templates are shown in Figure 4.

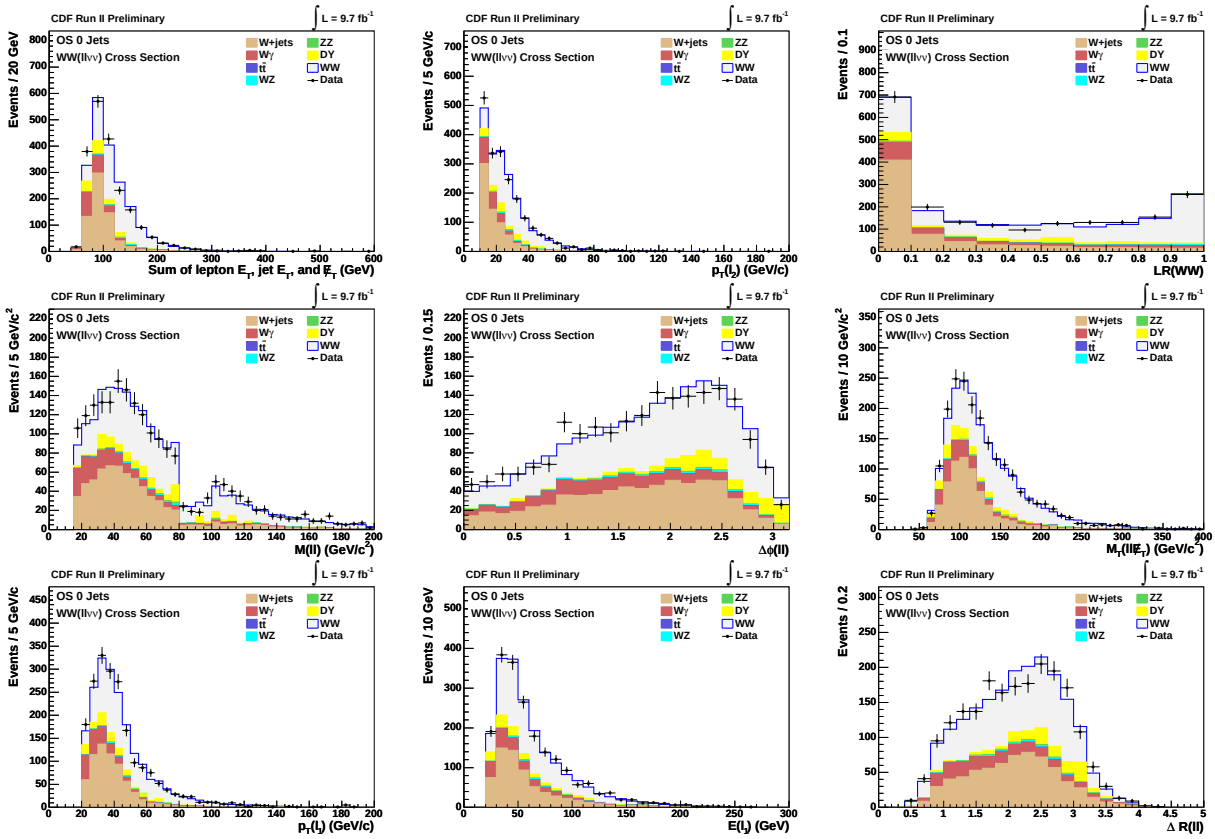

FIG. 2: 0 jet neural net inputs, ordered by significance

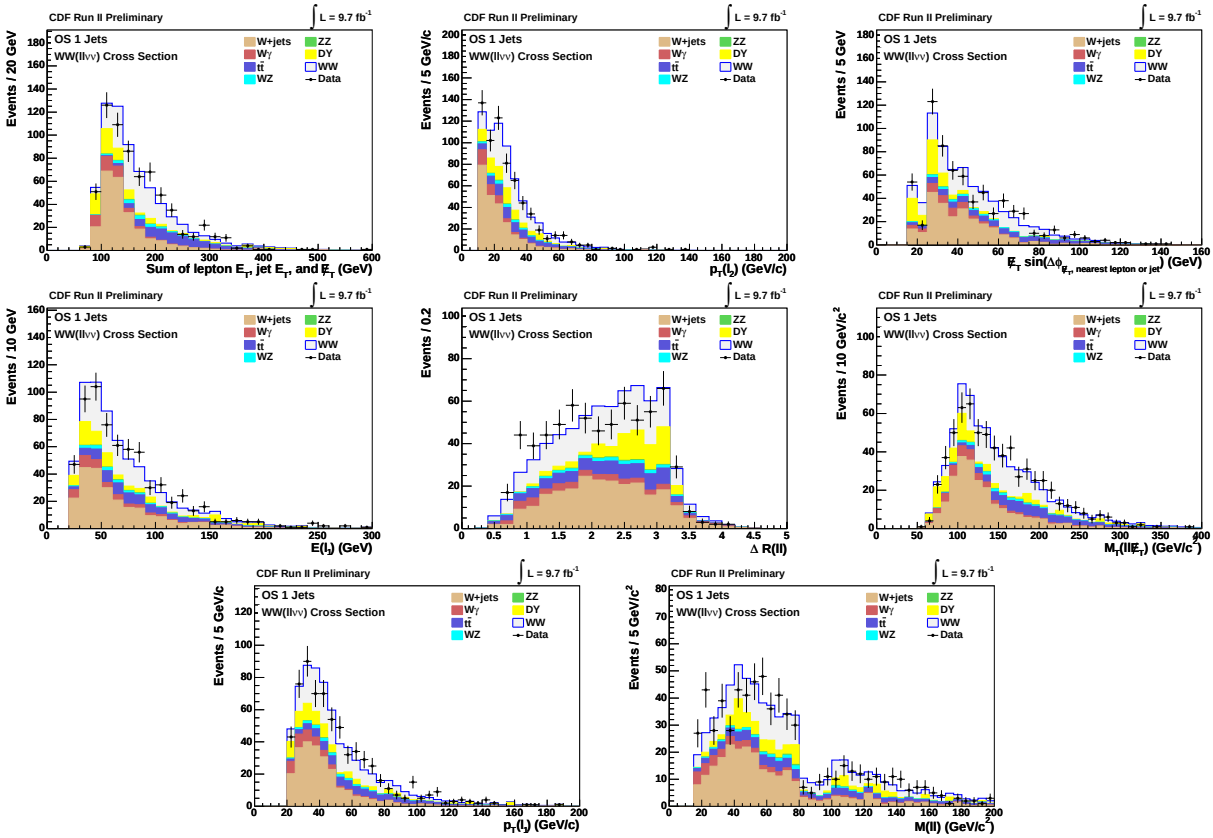

FIG. 3: 1 jet neural net inputs, ordered by significance

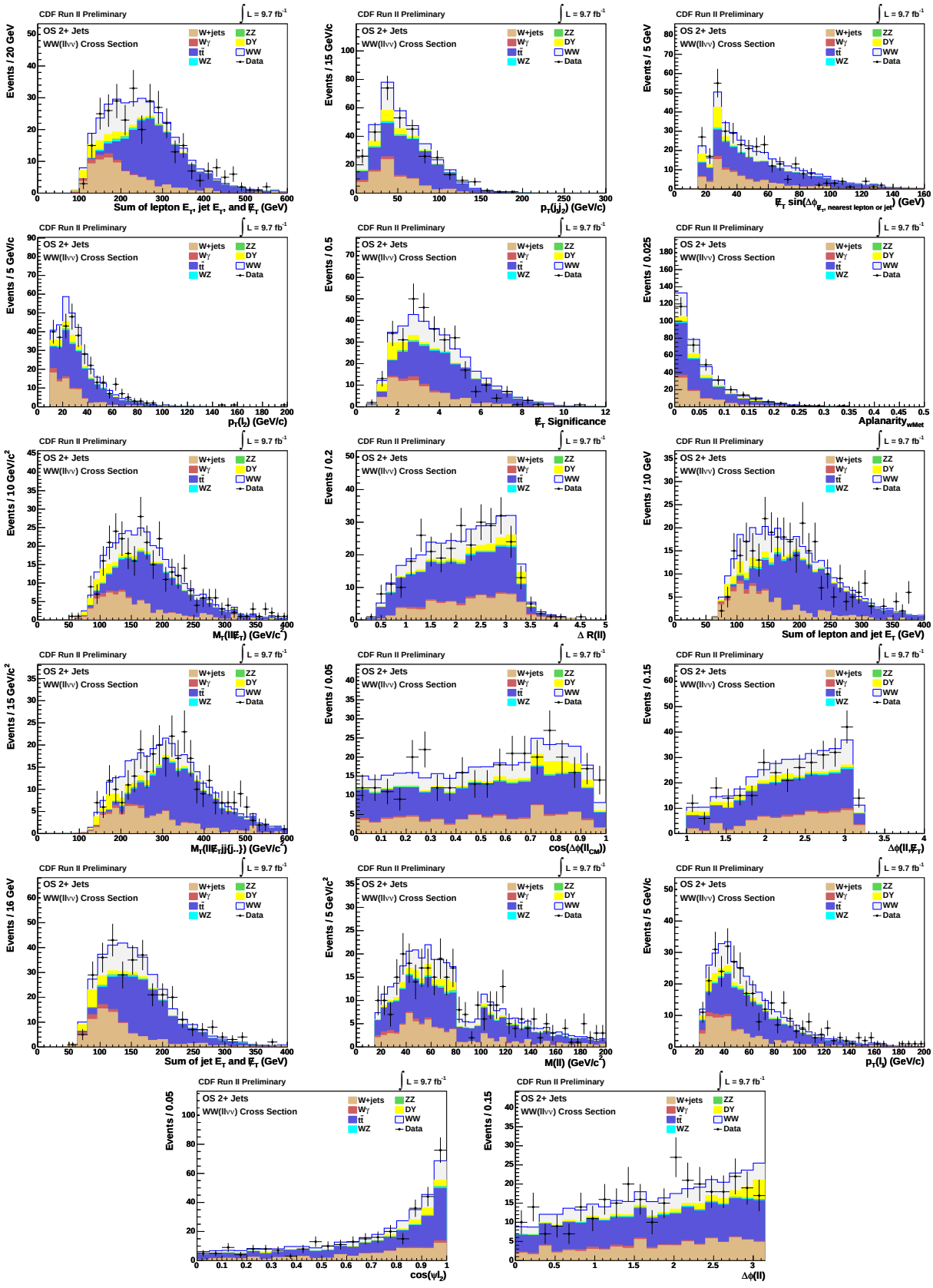

FIG. 4: 2 or more jet neural net inputs, ordered by significance

WW($\ell\ell\nu\nu$) Cross Section	0 Jets			CDF Run II Preliminary $\int \mathcal{L} = 9.7$ fb^{-1}			
Uncertainty Source	WW	WZ	ZZ	$t\bar{t}$	DY	$W\gamma$	W+jet
Cross Section	6.0%	6.0%	6.0%	4.3%*			
Acceptance							
$\not\!\!E_T$ Modeling					19.0%*		
Higher-order Diagrams		10.0%	10.0%			10.0%*	
$t\bar{t}$ QCD				2.7%			
Conversion Modeling						6.8%	
Scale	3.8%						
PDF Modeling	0.8%						
Jet Energy Scale	4.7%	6.4%	3.5%	26.8%	10.2%	3.5%	
Lepton ID Efficiencies	3.8%	3.8%	3.8%	3.8%	3.8%		
Trigger Efficiencies	2.0%	2.0%	2.0%	2.0%	2.0%		
Jet Fake Rate							17.2%
Luminosity	5.9%	5.9%	5.9%	5.9%	5.9%		

* indicates uncorrelated systematic. (−) indicates anticorrelated systematic.

TABLE II: systematic uncertainties used in the 0 jet analysis.

D. Systematic Uncertainties

We assess systematic uncertainties on the signal and background distributions arising from a wide variety of sources. systematic uncertainties include both rate uncertainties on expected event yields and shape uncertainties on expected event distributions.

We evaluate uncertainties on acceptance originating from lepton selection and trigger efficiency measurements, giving a 4.3% uncertainty on all event yields. We also assign acceptance uncertainties due to potential contributions from higher-order effects. For WW we evaluate acceptance uncertainty due to choice of showering scale by reweighting the Alpgen sample according to samples generated in Pythia 8[25] with varied showering scales. Varying the showering scale typically moves events between bins, and as a result the systematic is anti-correlated between the 0 and 1 jet low E_T bins and the higher bins, as indicated by the negative sign in the systematic uncertainties tables. Similarly, we evaluate acceptance uncertainty due to choie of PDF by reweighting the Alpgen sample according to MC@NLO samples generated with all 40 CTEQ6[16] error eigenvectors. A rate systematic is found to be negligible, and only a shape systematic is assessed.

For WZ and ZZ, which are simulated at leading order, we assign an uncertainty of 10%, the difference in the observed acceptance for WW between leading order (Pythia[24] and next-to-leading order (MC@NLO[17]). For $t\bar{t}$ we assign an uncertainty of 2.7% due to QCD effects taken from the dilepton $t\bar{t}$ cross section measurement[22], which uses similar Monte Carlo simulation and lepton selection. $W\gamma$ is generated with next-to-leading order Baur MC[2]. However, we assign a scale factor according to study of a low-m_{ll} control region to account for poor conversion modeling in the simulation. As extrapolation of this scale factor to the signal regions is dependent on background subtraction, we assign a 10% uncertainty to $W\gamma$ due to higher order diagrams, and a 6.8% uncertainty due to photon conversion modeling. The dominant systematic uncertainty on Drell-Yan is the modeling of fake $\not\!\!E_T$. In the zero and one jet bins, the $\not\!\!E_T$ modeling is tuned according to a control region with $\not\!\!E_T$ just below the signal selection threshold. An uncertainty of $19 - 26\%$ is assigned by varying the tuning. In the two jet region the tuning is found not to be needed. However, the uncertainty in modeling is kept. For all simulated backgrounds we vary the jet energy scale up and down by one standard deviation to determine the variation in acceptance for each process and region. We also assign a rate systematic for jet energy scale for WW and Drell-Yan. Because the effect of varying jet energy scale is to move events between bins, the systematic is anti-correlated between the zero and non-zero jet bins, as indicated by the negative sign in the systematic uncertainties tables.

For the W+jets background, the systematic uncertainty is determined from variation in the measured probabilities for a jet to be identified as a lepton using jet data collected at four different jet E_T trigger thresholds. The threshold affects both the parton composition of the jet and the relative amount of contamination from real leptons. Theoretical uncertainties on the cross section are assigned to $WW/WZ/ZZ$ (6%)[4][3] and $t\bar{t}$ (4.3%)[18]. The standard CDF luminosity uncertainty of 5.9%[13] has been assigned to all signal and background processes. The complete set of systematic uncertainties are summarized in Tables II-VI.

WW(ll$\nu\nu$) Cross Section	1 jet, $15 < E_T < 25$ GeV			CDF Run II Preliminary $\int \mathcal{L} = 9.7$ fb^{-1}			
Uncertainty Source	WW	WZ	ZZ	$t\bar{t}$	DY	$W\gamma$	W+jet
Cross Section	6.0%	6.0%	6.0%	4.3%*			
Acceptance							
$\not\!\!E_T$ Modeling					21.9%		
Higher-order Diagrams		10.0%	10.0%			10.0%*	
$t\bar{t}$ QCD				2.7%			
Conversion Modeling						6.8%	
Scale	0.5%						
PDF Modeling	1.2%						
Jet Energy Scale	−9.6%	−1.0%	−4.6%	−12.9%	−8.7%	−9.5%	
Lepton ID Efficiencies	3.8%	3.8%	3.8%	3.8%	3.8%		
Trigger Efficiencies	2.0%	2.0%	2.0%	2.0%	2.0%		
Jet Fake Rate							18.9%
Luminosity	5.9%	5.9%	5.9%	5.9%	5.9%		

* indicates uncorrelated systematic. (−) indicates anticorrelated systematic.

TABLE III: systematic uncertainties used in the 1 jet low E_T analysis.

WW(ll$\nu\nu$) Cross Section	1 jet, $25 < E_T < 45$ GeV			CDF Run II Preliminary $\int \mathcal{L} = 9.7$ fb^{-1}			
Uncertainty Source	WW	WZ	ZZ	$t\bar{t}$	DY	$W\gamma$	W+jet
Cross Section	6.0%	6.0%	6.0%	4.3%*			
Acceptance							
$\not\!\!E_T$ Modeling					22.1%		
Higher-order Diagrams		10.0%	10.0%			10.0%*	
$t\bar{t}$ QCD				2.7%			
Conversion Modeling						6.8%	
Scale	−5.6%						
PDF Modeling	1.2%						
Jet Energy Scale	−5.8%	−1.0%	−4.6%	−12.9%	−22.9%	−9.5%	
Lepton ID Efficiencies	3.8%	3.8%	3.8%	3.8%	3.8%		
Trigger Efficiencies	2.0%	2.0%	2.0%	2.0%	2.0%		
Jet Fake Rate							18.9%
Luminosity	5.9%	5.9%	5.9%	5.9%	5.9%		

* indicates uncorrelated systematic. (−) indicates anticorrelated systematic.

TABLE IV: systematic uncertainties used in the 1 jet mid E_T analysis.

E. Results

We extract the differential WW cross section from the neural net output shapes, estimated normalizations, and systematic uncertainties of signal and background in each signal region via a binned maximum likelihood method. The systematic uncertainties are subject to a Gaussian constraint, while the signal normalization in each region is allowed to float freely. Shape systematic uncertainties are evaluated via vertical interpolation. The fitted neural net output templates are shown in Figures 6-11. The result is unfolded to the hadronic level based on the results of a study of the bin to bin migration of events due to jet reconstruction, scale, and resolution effects as determined by comparing hadron jet clustered Monte Carlo events to fully simulated and reconstructed Monte Carlo events. The final result is iteratively corrected to account for differences in acceptance between the reconstructed and true distributions using a Bayesian method implemented in RooUnfold[1]. In order to quantify our expectations we generate 10,000 pseudoexperiments, each of which is minimized exactly as data. The minimum values of the negative log likelihood for both pseudoexperiments and data are shown in Figure 5. The fit gives a measured value of $14.0 \pm 0.6(stat)^{+1.6}_{-1.3}(syst) \pm 0.8(lumi)$ for the inclusive cross section. This is slightly higher than the predictions of Alpgen(11.3 ± 1.4) and MC@NLO(11.7 ± 0.9) but consistent with both predictions. Predictions, measured values, and scale factors for the differential and inclusive cross section are listed in Table VII and shown in Figure 12. The results are consistently high but within one standard deviation, except for the two or more jet bin, which is within two standard deviations.

WW($ll\nu\nu$) Cross Section	1 jet, $E_T > 45$ GeV			CDF Run II Preliminary $\int \mathcal{L} = 9.7$ fb^{-1}			
Uncertainty Source	WW	WZ	ZZ	$t\bar{t}$	DY	$W\gamma$	W+jet
Cross Section	6.0%	6.0%	6.0%	4.3%*			
Acceptance							
$\not\!\!E_T$ Modeling					23.0%		
Higher-order Diagrams		10.0%	10.0%			10.0%*	
$t\bar{t}$ QCD				2.7%			
Conversion Modeling						6.8%	
Scale	−23.7%						
PDF Modeling	1.3%						
Jet Energy Scale	−2.7%	−1.0%	−4.6%	−12.9%	3.7%	−9.5%	
Lepton ID Efficiencies	3.8%	3.8%	3.8%	3.8%	3.8%		
Trigger Efficiencies	2.0%	2.0%	2.0%	2.0%	2.0%		
Jet Fake Rate							18.9%
Luminosity	5.9%	5.9%	5.9%	5.9%	5.9%		

* indicates uncorrelated systematic. (−) indicates anticorrelated systematic.

TABLE V: systematic uncertainties used in the 1 jet high E_T analysis.

WW($ll\nu\nu$) Cross Section	2 or More Jets			CDF Run II Preliminary $\int \mathcal{L} = 9.7$ fb^{-1}			
Uncertainty Source	WW	WZ	ZZ	$t\bar{t}$	DY	$W\gamma$	W+jet
Cross Section	6.0%	6.0%	6.0%	4.3%*			
Acceptance							
$\not\!\!E_T$ Modeling					26.0%*		
Higher-order Diagrams		10.0%	10.0%			10.0%*	
$t\bar{t}$ QCD				2.7%			
Conversion Modeling						6.8%	
Scale	−13.0%						
PDF Modeling	1.8%						
Jet Energy Scale	−21.5%	−13.2%	−13.3%	−1.7%	−28.7%	−22.0%	
Lepton ID Efficiencies	3.8%	3.8%	3.8%	3.8%	3.8%		
Trigger Efficiencies	2.0%	2.0%	2.0%	2.0%	2.0%		
Jet Fake Rate							19.0%
Luminosity	5.9%	5.9%	5.9%	5.9%	5.9%		

* indicates uncorrelated systematic. (−) indicates anticorrelated systematic.

TABLE VI: systematic uncertainties used in the 2 jet analysis.

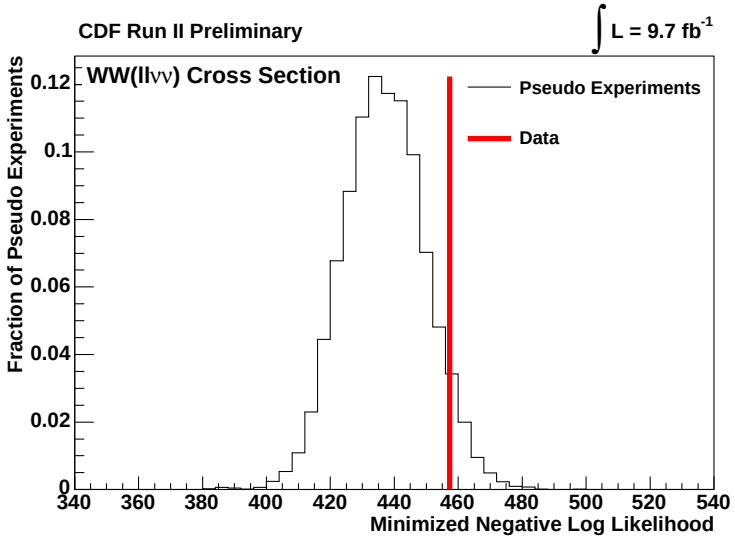

FIG. 5: Distribution of minimized negative log likelihood for 10,000 pseudo-experiments and for data (indicated by red line).

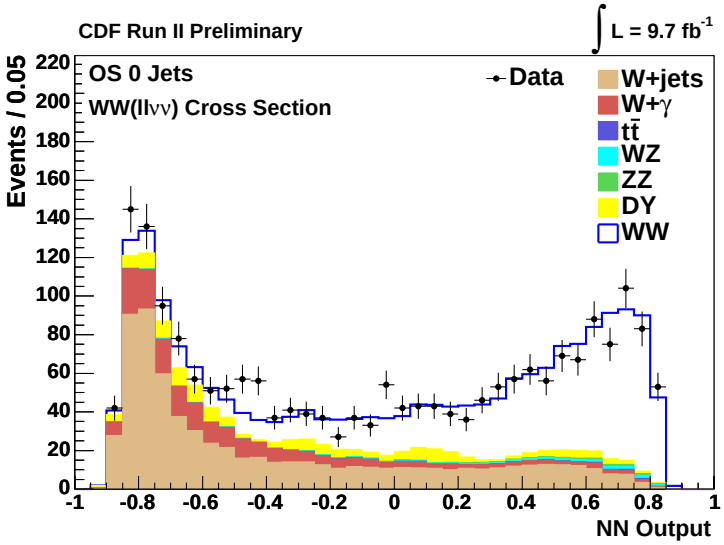

FIG. 6: Templates after fitting in the 0 jet bin.

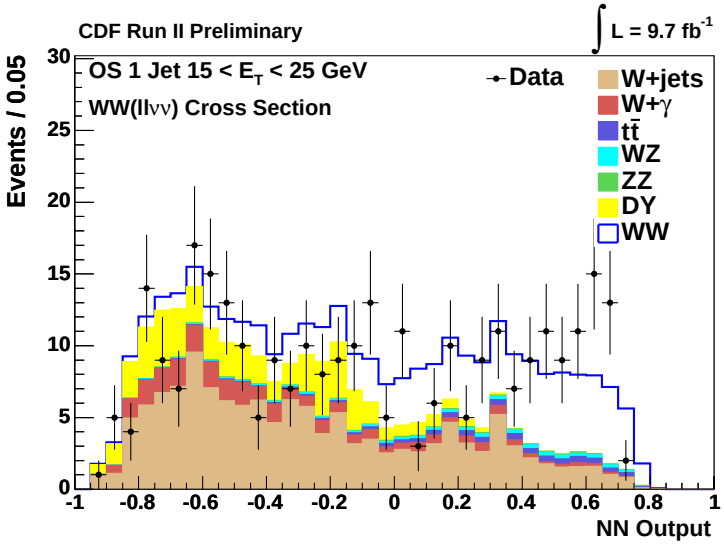

FIG. 7: Templates after fitting in the one jet low E_T bin.

WW(ll$\nu\nu$) Cross Section	CDF Run II Preliminary			$\int \mathcal{L} = 9.7$ fb^{-1}	
	σ(pb)	Uncertainty(pb)			σ(pb)	
Jet Bin	Measured	Stat.	Syst.	Lumi.	Alpgen	MC@NLO
Inclusive	14.0	± 0.6	$^{+1.6}_{-1.3}$	± 0.8	11.3 ± 1.4	11.7 ± 0.9
0 Jets	9.6	± 0.4	$^{+1.1}_{-0.9}$	± 0.6	8.2 ± 1.0	8.6 ± 0.6
1 Jet Inclusive	3.05	± 0.46	$^{+0.48}_{-0.32}$	± 0.18	2.43 ± 0.31	2.47 ± 0.18
1 jet, $15 < E_T < 25$ GeV	1.47	± 0.17	$^{+0.15}_{-0.11}$	± 0.09	1.26 ± 0.16	1.18 ± 0.09
1 jet, $25 < E_T < 45$ GeV	1.09	± 0.18	$^{+0.17}_{-0.12}$	± 0.06	0.77 ± 0.10	0.79 ± 0.06
1 jet, $E_T > 45$ GeV	0.49	± 0.15	$^{+0.20}_{-0.11}$	± 0.03	0.40 ± 0.05	0.46 ± 0.03
2 or More jets	1.36	± 0.30	$^{+0.46}_{-0.29}$	± 0.08	0.64 ± 0.08	0.61 ± 0.05

TABLE VII: Table of inclusive and differential cross section measurements and predictions

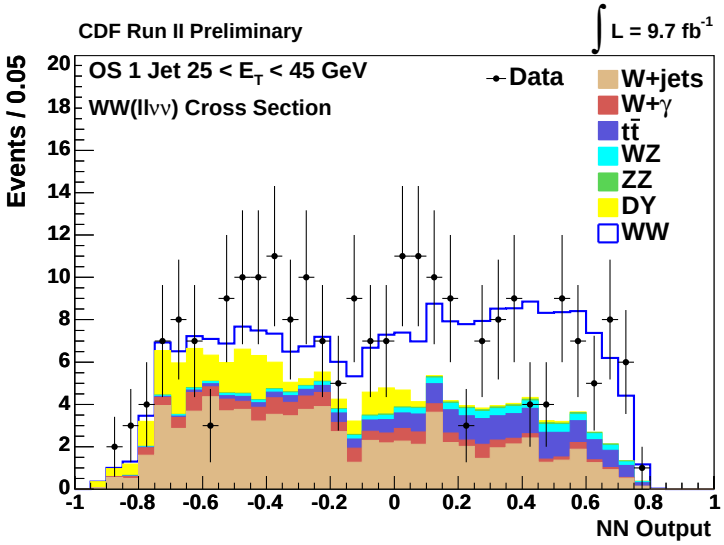

FIG. 8: Templates after fitting in the one jet intermediate E_T bin.

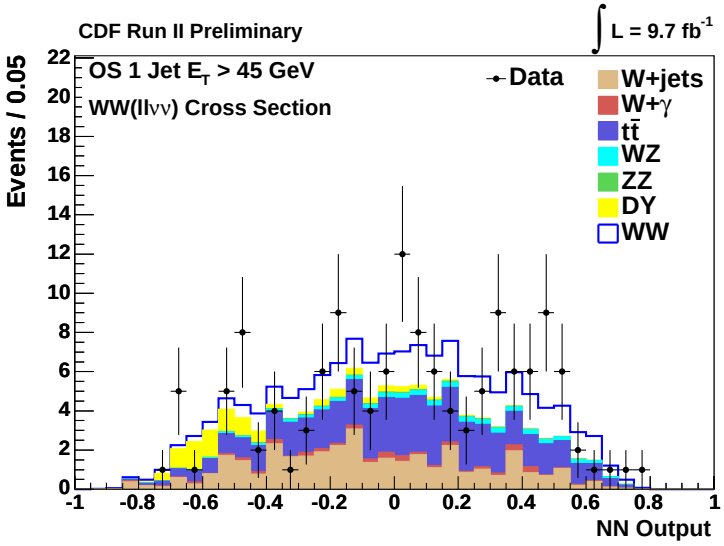

FIG. 9: Templates after fitting in the one jet high E_T bin.

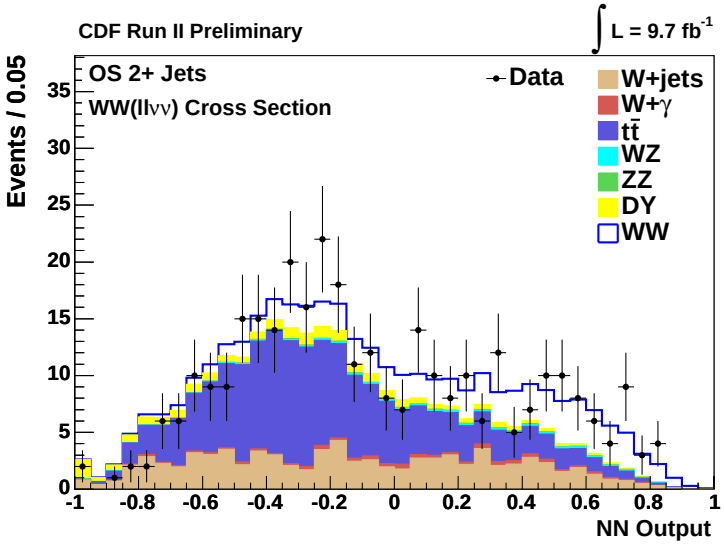

FIG. 10: Templates after fitting in the two or more jet bin.

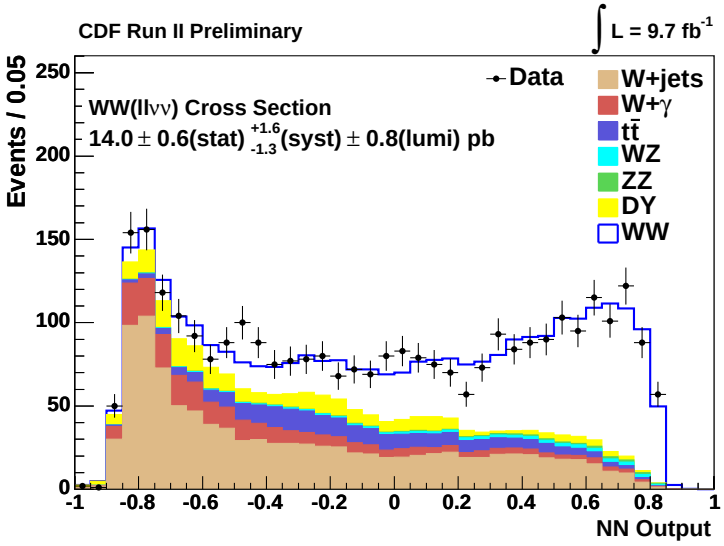

FIG. 11: Templates after fitting for all data.

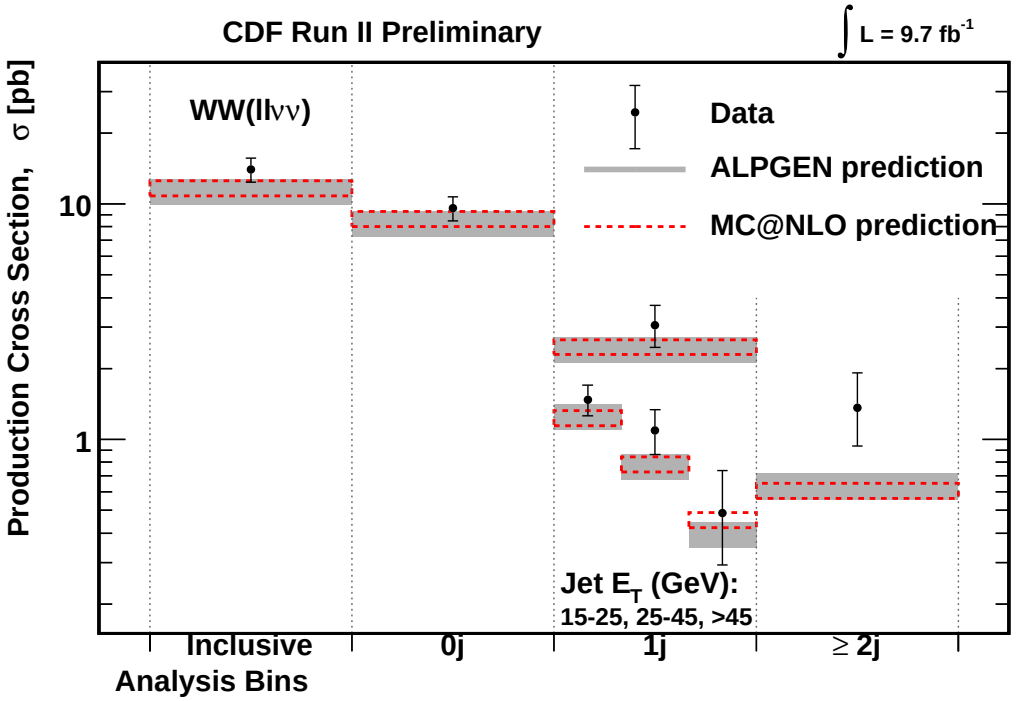

FIG. 12: Inclusive and differential cross section measurements and predictions.

VIII. CONCLUSION

We have measured the WW cross section, both inclusive and differential in jet multiplicity and E_T, using a neural network discriminant and maximum likelihood fit. The measured cross section, $14.0 \pm 0.6(stat)^{+1.6}_{-1.3}(syst) \pm 0.8(lumi)$, is consistent with the Standard Model prediction. This is the most precise measurement of the WW cross section at a $p\bar{p}$ collider, and the first differential cross section measurement in a massive diboson state.

[1] T. Adye. Unfolding algorithms and tests using roounfold, 2011. data-an/1105.1160.
[2] U. Baur and E. L. Berger. *Phys. Rev. D*, 47(4889), 1993.
[3] J. M. Campbel and R. K. Ellis. *Phys. Rev. D*, 60(113006), 1999. hep-ph/9905386.
[4] J. Campbell and K. Ellis. Mcfm - monte carlo for femtobarn processes, 2005. http://mcfm.fnal.gov/.
[5] ATLAS Collaboration. Measurement of the w^+w^- cross sections in $\sqrt{s} = 7$ tev pp collisions with the atlas detector and limits on anomalous gauge couplings. *Physics Letters B*, 712(4-5), 2012.
[6] CDF Collaboration. Measurement of the w^+w^- production cross section and search for anomalous $ww\gamma$ and wwz couplings in $p\bar{p}$ collisions at $\sqrt{s} = 1.96$ tev journal =.
[7] CDF Collaboration. The cdf-ii detector: Technical design report, 1996. FERMILAB-DESIGN-1996, FERMILAB-PUB-96-390-E.
[8] CDF Collaboration. *Nucl. Instrum. Methods A*, 447(1), 2000.
[9] CDF Collaboration. *Nucl. Instrum. Methods A*, 453(84), 2000.
[10] CDF Collaboration. *Nucl. Instrum. Methods A*, 526(249), 2004.
[11] CMS Collaboration. Measurement of the w^+w^- and zz production cross sections in pp collisions at $\sqrt{s} = 8$ tev. *Physics Letters B*, 721(4-5), 2013.
[12] D0 Collaboration. Measurement of the ww production cross section with dilepton final states in $p\bar{p}$ collisions at $\sqrt{s} = 1.96$ tev and limits on the anomalous trilinear gauge couplings. *Physical Review Letters*, 103(191801), 2009.
[13] (CDF Collaboration) D. Acosta et al. *Nucl. Instrum. Methods A*, 494(57), 2002.
[14] S. Oh G. Yu P. M. Fernandez E. James S. Jindariani T. Junk et al. D. Benjamin, M. Kruse. Search for h to ww production using 9.7 fb-1, 2012. CDF/PUB/EXOTIC/PUBLIC/10785.
[15] H. L. Lai et al. Global qcd analysis of parton structure of the nucleus: Cteq5 parton distributions. *The European Physical Journal C*, 12(3), 2000.
[16] P. Nadolsky et al. *Phys. Rev. D*, 78(013004), 2008.
[17] S. Frixione and B. R. Webber. *JHEP*, 0206(029), 2002.
[18] P. Fiedler M. Czakon and A. Mitov. Total top-quark pair-production cross section at hadron colliders through $o(\alpha_s^4)$. *Phys. Rev. Lett.*, 110(252004), 2013.
[19] F. Piccinini R. Pittau A. D. Polosa M. L. Mangano, M. Moretti. Alpgen, a generator for hard multiparton processes in hadronic collisions. *JHEP*, 0307(001), 2003.
[20] M. Hansroul J.C.Lassalle R. Brun, R. Hagelberg. Geant: Simulation program for particle physics experiments. user guide and reference manual, 1978. CERN-DD-78-2-REV, CERN-DD-78-2.
[21] (CDF Collaboration) T. Aaltonen et al. Searches for the higgs boson decaying to $w^+w^- \to l^+\nu l^-\bar{\nu}$ with the cdf ii detector. *Physical Review D*, 88(052012), 2013.
[22] (CDF Collaboration) T. Aaltonen et al. Combination of measurements of the top-quark pair production cross section from the tevatron collider. *Phys. Rev. D*, 89(072001), 2014.
[23] T. Junk M. Kirby R. Snider et al. T. Phillips, J. Freeman. Introduction to hobit, a b jet identification tagger at the cdf experiment optimized for light higgs searches, 2012. CDF/DOC/CDF/PUBLIC/10803.
[24] L. Lonnblad T. Sjostrand and S. Mrenna, 2001. hep-ph/0108264.
[25] S. Mrenna T. Sjostrand and P. Skands. *JHEP05*, 026, 2006. Comput. Phys. Comm. 178 (2008) 852.